International Journal of Thin Films Science and Technology

http://dx.doi.org/10.18576/ijtfst/150205

Recycling Spent Batteries into High-Efficiency MoS_2@GO Composites for Phenol Removal from Aqueous Solutions

Mohammad A. M. Ali [1], *Abdelrahman M. Hamed* [1], *Gomaa A. M. Ali* [2,*], *Zinab H. Bakr* [2,3], *Abdelaal S. A. Ahmed* [1,*]

[1] Chemistry Department, Faculty of Science, Al-Azhar University, Assiut 71524, Egypt
[2] Sharjah Marine Science Research Centre, College of Marine Science and Aquatic Biology, University of Khorfakkan, Khorfakkan, 18119, Sharjah, United Arab Emirates
[3] Physics Department, Faculty of Science, Assiut University, Assiut, 71516, Egypt

Received: 1 Feb. 2026, Revised: 10 Mar. 2026, Accepted: 19 Apr. 2026
Published online: 1 May 2026

Abstract: This work presents the preparation of carbon (C), MoS_2@C, and MoS_2@graphene oxide (GO) composites derived from spent batteries for the efficient removal of phenol from aqueous solutions. The physicochemical properties of the synthesized materials were characterized using Fourier transform infrared spectroscopy (FTIR), X-ray diffraction (XRD), and transmission electron microscopy (TEM). The adsorption performance was systematically evaluated through batch experiments by examining the effects of solution pH, contact time, initial phenol concentration, and temperature. Among the investigated adsorbents, the MoS_2@GO composite exhibited the highest adsorption performance, achieving a phenol removal efficiency of 96% within 120 min. Kinetic analysis showed that the adsorption data were best described by the pseudo-second-order model, whereas the equilibrium data were in good agreement with the Langmuir isotherm, indicating monolayer adsorption on homogeneous active sites. The maximum adsorption capacities of C, MoS_2@C, and MoS_2@GO were determined to be 13.05, 16.28, and 20.25 mg/g, respectively. Thermodynamic evaluation revealed that the adsorption process was exothermic, while the calculated Gibbs free energy values indicated that adsorption was thermodynamically non-spontaneous under the investigated conditions. In addition, the prepared composites retained satisfactory adsorption performance during regeneration experiments, demonstrating good reusability. These findings highlight the potential of MoS_2@GO synthesized from spent batteries as an environmentally sustainable and economically attractive adsorbent for the treatment of phenol-contaminated wastewater.

Keywords: Wastewater Treatment; Adsorption; 2D Nanomaterials; Recycling; Phenol; Environmental Pollution; Sustainability.

1 Introduction

The increasing contamination of water resources has become one of the most serious environmental challenges due to its adverse impacts on ecosystems and public health. Rapid industrialization and agricultural activities release a wide range of organic and inorganic contaminants into aquatic environments, making efficient wastewater treatment essential before discharge [1,2,3]. Among these pollutants, phenol and its derivatives are frequently detected in effluents from petroleum refineries, resin manufacturing, pharmaceutical industries, dye production, plastics, and other chemical processes. Because of their persistence, toxicity, and resistance to biodegradation, phenolic compounds are classified as priority pollutants and are subject to stringent environmental regulations [4,5].

Numerous treatment technologies have been developed for the removal of phenol from wastewater, including biological degradation, membrane filtration, catalytic oxidation, and advanced oxidation processes [6,7,8]. Although these techniques can effectively reduce phenol concentrations, many suffer from drawbacks such as high operational costs, complicated treatment processes, and limited efficiency under certain operating conditions. Consequently, adsorption has emerged as one of the most attractive alternatives owing to its high removal efficiency, operational simplicity, low energy consumption, and environmental compatibility. Furthermore, adsorption minimizes the formation of secondary pollutants and can be readily implemented in large-scale wastewater treatment systems [9,10]. The effectiveness of an adsorption process is strongly dependent on the physicochemical properties of

* Corresponding author e-mail: abdelaalsaiyd@azhar.edu.eg ; gomaa.ali@ukf.ac.ae

the adsorbent. Therefore, considerable research has been devoted to developing highly efficient and economically viable adsorbent materials. Conventional adsorbents such as activated carbon, clays, zeolites, and metal oxides have demonstrated excellent adsorption capacities. More recently, advanced materials, including metal-organic frameworks (MOFs), two-dimensional (2D) materials, metal phosphides, and biomass-derived carbons, have attracted increasing attention because of their unique structural characteristics and enhanced adsorption performance [11, 12, 13, 14]. However, the relatively high production cost of many commercial adsorbents limits their widespread practical application. Consequently, the conversion of waste materials into value-added adsorbents has become an attractive and sustainable strategy that simultaneously addresses waste management and environmental remediation [15, 16].

Spent Eveready carbon dry-cell batteries constitute an abundant source of carbonaceous materials that can be recycled into functional adsorbents, thereby promoting sustainable resource utilization while reducing environmental pollution. Among the emerging adsorbent materials, molybdenum disulfide (MoS_2) has attracted considerable attention because of its layered structure, abundant exposed edge sites, and favorable physicochemical properties for the adsorption of organic pollutants [17]. Nevertheless, pristine MoS_2 is prone to aggregation during synthesis, which reduces the accessibility of its active sites and consequently limits its adsorption performance. To overcome this limitation, carbonaceous materials and graphene oxide (GO) have been widely employed as supporting matrices to improve the dispersion, stability, and accessibility of MoS_2 nanosheets. In particular, GO possesses a high specific surface area and abundant oxygen-containing functional groups that provide additional adsorption sites and facilitate hydrogen bonding and π-π interactions with aromatic pollutants such as phenol.

Although MoS_2, GO, and MoS_2/GO-based adsorbents have been extensively investigated for wastewater treatment, most reported studies have utilized commercially available graphite or synthetic carbon materials as the supporting matrix. In contrast, the utilization of recycled carbon recovered from spent batteries for the preparation of MoS_2-based composites remains largely unexplored. Therefore, developing sustainable adsorbents that combine waste valorization with high adsorption performance represents an important research challenge. The present study addresses this gap by employing recycled carbon recovered from spent Eveready carbon batteries as a precursor for the synthesis of MoS_2@C and MoS_2@GO composites through a hydrothermal method. The novelty of this work lies in integrating battery waste recycling with the fabrication of efficient adsorbents and systematically evaluating their adsorption performance toward phenol through adsorption kinetics, equilibrium isotherms, thermodynamic analysis, and regeneration studies. This approach not only offers an environmentally friendly route for recycling spent batteries but also demonstrates the potential of recycled carbon-based MoS_2 composites as sustainable and cost-effective adsorbents for wastewater treatment.

The adsorption performance of the prepared materials toward phenol was systematically evaluated by investigating the effects of solution pH, contact time, adsorbent dosage, initial phenol concentration, and temperature. In addition, adsorption kinetics, equilibrium isotherms, thermodynamic parameters, and regeneration behavior were analyzed to provide a comprehensive understanding of the adsorption process. The results demonstrate that the recycled MoS_2@GO composite exhibits superior adsorption efficiency compared with recycled carbon and the MoS_2@C composite, highlighting its potential as an efficient and sustainable adsorbent for phenol removal from contaminated water.

2 Experimental procedures

2.1 Chemicals and Reagents

All chemicals used in this study were of analytical grade and were used without further purification. Sulfuric acid (H_2SO_4, 95%), ammonium hydroxide (NH_4OH, 28% NH_3 in H_2O), potassium permanganate ($KMnO_4$, 97%), sodium hydroxide (NaOH, $\geq$ 98%, anhydrous), sodium nitrate ($NaNO_3$, $\geq$ 99.0%), hydrochloric acid (HCl, 37%), hydrogen peroxide (H_2O_2, 30% w/w in water), and absolute ethanol (C_2H_5OH, $\geq$ 95%) were purchased from Merck (Darmstadt, Germany). Phenol (C_6H_5OH, $\geq$ 99%) and ammonium heptamolybdate tetrahydrate ($(NH_4)_6Mo_7O_{24} \cdot 4H_2O$, 99.98% trace metals basis) were obtained from Sigma-Aldrich. All solutions and preparations were made using distilled water.

2.2 Synthesis of adsorbents

Three carbon-based adsorbents were prepared in this study, namely recycled carbon (C), MoS_2@C, and MoS_2@GO composites. GO was synthesized from graphite rods recovered from spent Eveready dry-cell batteries using the modified Hummers method [16]. Prior to dismantling, the batteries were completely discharged to ensure safe handling. The graphite rods were manually separated, thoroughly washed with deionized water to remove residual electrolyte and impurities, dried, and ground into a fine powder.

For GO synthesis, 1.0 g of graphite powder was mixed with 1.0 g of $NaNO_3$, followed by the gradual addition of 23 mL of concentrated H_2SO_4 under continuous stirring in an ice bath. Subsequently, 3.0 g of $KMnO_4$ was slowly added while maintaining the temperature below 20 °C. The mixture was then stirred at 40 °C for 2 h. Afterwards, 50 mL of distilled water was carefully added, followed by 12 mL of H_2O_2 to terminate the oxidation reaction. After dilution with 260 mL of distilled water, the product was collected by centrifugation, repeatedly washed with distilled water until neutral pH was achieved, and dried at 100 °C for 24 h.

The MoS_2@C and MoS_2@GO composites were synthesized by a hydrothermal method adapted from previ-

ously reported procedures [11,18]. Under hydrothermal conditions, thiourea gradually decomposes to generate sulfur-containing species (H_2S/S^{2-}), which react with the molybdenum precursor to form MoS_2 nanosheets. Simultaneously, thiourea facilitates the reduction of Mo(VI) to Mo(IV), promoting the formation of crystalline MoS_2 uniformly on the carbonaceous supports [19].

For the synthesis of the MoS_2@C composite, 0.20 g of recycled carbon was dispersed in 50 mL of distilled water and stirred for 1 h. An aqueous solution containing 0.26 g of ammonium heptamolybdate dissolved in 30 mL of distilled water was then added, followed by stirring for 20 min. Subsequently, an aqueous solution containing 2.5 g of thiourea dissolved in 20 mL of distilled water was introduced, and the mixture was stirred for an additional 1 h. The resulting suspension was transferred into a 100 mL Teflon-lined stainless-steel autoclave and heated at 180 °C for 24 h. After cooling to room temperature, the product was collected, washed, dried, and denoted as MoS_2@C. The MoS_2@GO composite was synthesized using the same hydrothermal procedure, with GO replacing recycled carbon as the supporting material. During the hydrothermal treatment, MoS_2 nanosheets nucleated and grew directly on the GO sheets, producing the MoS_2@GO composite through strong interfacial interactions between MoS_2 and the oxygen-containing functional groups of GO.

2.3 Characterization

The crystallinity of the materials was investigated by X-ray diffraction (XRD) using a Bruker D8 advanced X-ray diffractometer (monochromatic Cu-Kα radiation source, λ=0.15406 nm) running at 40 kV. Functional groups were identified through Fourier-transform infrared spectroscopy (FTIR). The FTIR spectrum was recorded in the 4000-400 cm^{-1} region at a resolution of 2 cm^{-1} on a Nicolet spectrophotometer (model 6700) by using the KBr pellet technique. The surface morphology and microstructure were evaluated using a field emission scanning electron microscope (SEM, JSM-6610, JEOL, Japan) and a transmission electron microscope (TEM, JEM-2100F, JEOL, Japan) operating at an accelerating voltage of 200 kV. The concentration of NH_4^+ ions in solution was measured using a spectrophotometric method.

2.4 Adsorption Study

Phenol adsorption was carried out in a 300 mL flask under a magnetic stirrer. Using the batch adsorption method, the effects of solution pH (2-12), contact time (10-120 min), adsorbent dosages, and initial phenol concentration (10-200 mg/L) on the adsorption effectiveness of the produced C, MoS_2@C, and MoS_2@GO materials were examined. In each experiment, 20 mL of phenol solution was mixed with 0.05 g of individual materials and agitated for varying contact times. 0.1 M HCl and 0.1 M NaOH solutions were used to change the pH of the solution. After the adsorption experiment, the suspensions were centrifuged to separate the adsorbent. An aliquot of the clear supernatant was mixed with $FeCl_3$ solution to develop the characteristic violet ferric-phenolate complex. After allowing sufficient time for colour development (e.g., 5-10 min), the absorbance was measured at 540 nm using a Hitachi UV-2900 UV-Vis spectrophotometer against a reagent blank. The residual phenol concentration was determined from a calibration curve prepared using standard phenol solutions treated under identical conditions. The removal percentage (R%) was calculated using Eq. 1 [13]:

$$R\,(\%) = \frac{C_i - C_f}{C_i} \times 100 \tag{1}$$

The amount of phenol adsorbed qe (mg/g) was calculated from the mass balance equation as given by Eq. 2.

$$q_e = \frac{(C_i - C_f)}{W} V \tag{2}$$

Where Ci and Cf are the initial and equilibrium phenol concentrations, respectively. W (g) is the mass of adsorbent, and V is the phenol volume (L).

2.5 Adsorbents regeneration

Desorption experiments were conducted to evaluate the reusability of the C, MoS_2@C, and MoS_2@GO composites. Briefly, 0.1 g of each adsorbent was mixed with 20 mL of a 50 mg/L phenol solution and magnetically stirred for 90 min at 25 °C. After adsorption, the phenol-loaded adsorbents were separated by centrifugation, dried, and then immersed in 20 mL of 0.1 M NaOH solution. The suspension was magnetically stirred for 90 min at 25 °C to facilitate the adsorption of phenol. No sonication or external heating was applied during the desorption process. After desorption, the solution was separated from the regenerated adsorbent, and the concentration of desorbed phenol was determined. The regenerated adsorbents were subsequently washed several times with deionized water until neutral pH, dried, and reused in the next adsorption cycle. The adsorption-desorption procedure was repeated for five consecutive cycles to evaluate the reusability of the prepared adsorbents. All adsorption experiments were performed in triplicate under identical experimental conditions.

3 Results And Discussion

3.1 Characterization of the adsorbents

The XRD patterns of the prepared materials are presented in Fig. 1. The diffraction pattern of the recycled carbon (Fig. 1a) exhibits diffraction peaks at 2θ values of 18.45°, 20.85°, 23.56°, 40.19°, 42.71°, 53.24°, 72.51°, and 77.43°, corresponding to the (111), (200), (210), (321), (400), (430), (540), and (542) crystallographic planes, respectively. The XRD pattern of the MoS_2@C composite (Fig. 1b) displays diffraction peaks at 2θ = 5.73°, 18.21°, 23.50°, 32.70°, 46.30°, and 56.00°, which can be indexed to the (111), (333), (550), (102), (006), and (110) planes of hexagonal 2H-MoS_2 (JCPDS No. 37-1492) [20]. The observed broad diffraction peaks indicate the nanocrystalline nature of the deposited MoS_2 and suggest the formation of few-layer MoS_2 nanosheets on the recycled carbon support. No additional diffraction peaks

corresponding to impurity phases were detected, indicating the successful formation of the MoS_2 phase.

For the MoS_2@GO composite (Fig. 1c), diffraction peaks were observed at 2θ = 20.58°, 38.13°, 46.80°, 60.19°, 64.98°, and 76.71°, which are indexed to the (111), (103), (123), (224), (333), and (442) planes, respectively. Compared with the MoS_2@C composite, several MoS_2 diffraction peaks exhibit lower intensity or become less distinguishable. This behavior is attributed to the high dispersion of few-layer MoS_2 on the GO sheets, together with the relatively low MoS_2 loading and reduced crystallite size, which decrease the diffraction intensity. These observations are consistent with the formation of well-dispersed MoS_2 nanosheets on the GO support without evidence of undesirable crystalline impurity phases.

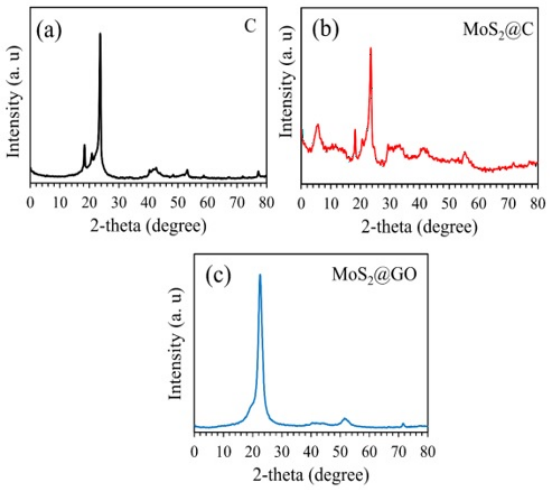

Fig. 1: XRD of (a) C, (b) MoS_2@C, and (c) MoS_2@GO composites.

The FTIR spectra of the prepared materials are presented in Fig. 2. The spectrum of C (Fig. 2a) exhibits a broad absorption band centered at 3500 cm^{-1}, which is attributed to the O–H stretching vibration of hydroxyl groups and adsorbed water molecules. The bands observed at 2919-3000 cm^{-1} correspond to the stretching vibrations of aliphatic C–H bonds.

For the MoS_2@C composite (Fig. 2b), the absorption band at 1379 cm^{-1} is assigned to aliphatic C–H bending vibrations, while the bands between 1399 and 1022 cm^{-1} are attributed to C–O stretching vibrations of oxygen-containing surface functional groups, including carboxyl species. These oxygen-containing functionalities are likely formed through the partial oxidation of the recycled carbon during battery use, sample purification, and the hydrothermal synthesis process. Such surface groups are commonly present on defect-rich carbon materials and promote the anchoring of MoS_2 nanoparticles while providing additional adsorption sites for phenol molecules. The characteristic absorption bands observed at 2100, 1650, 1390, and 1140 cm^{-1} are consistent with those reported for MoS_2.

The FTIR spectrum of the MoS_2@GO composite (Fig. 2c) displays the characteristic functional groups of GO and MoS_2. A broad absorption band at 3413 cm^{-1} is assigned to the O–H stretching vibration of hydroxyl groups and adsorbed water molecules. The band at 1716 cm^{-1} corresponds to the stretching vibration of carbonyl (C=O) groups, while the peak at 1576 cm^{-1} is attributed to the skeletal vibration of graphitic C=C bonds. The bands between 1399 and 1022 cm^{-1} are assigned to C–O stretching vibrations of oxygen-containing functional groups. These surface functional groups, together with the graphitic carbon framework and MoS_2 active sites, are expected to enhance phenol adsorption through hydrogen bonding, π-π interactions and van der Waals interactions.

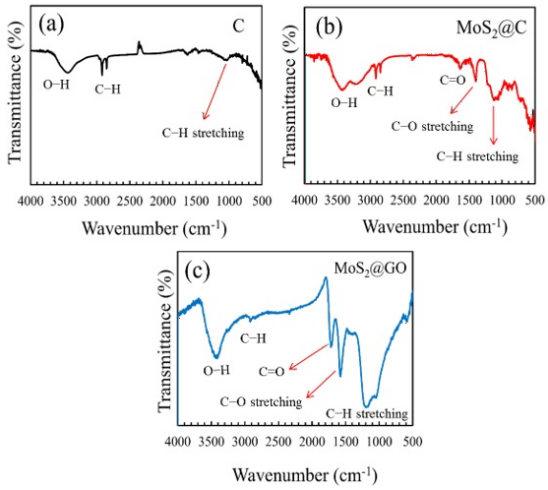

Fig. 2: FTIR of (a) C, (b) MoS_2@C, and (c) MoS_2@GO composites.

The morphology of the prepared MoS_2@C and MoS_2@GO composite materials was investigated using TEM, and the images are presented in Fig. 3. The TEM images reveal that both composites exhibit irregular and aggregated morphologies, which are commonly observed for hydrothermally synthesized carbon-based and MoS_2-based nanomaterials. For the MoS_2@C composite, the TEM images before phenol adsorption (Fig. 3a) display large, aggregated, non-uniform particles composed of smaller primary units clustered together to form irregular agglomerates. In contrast, after phenol adsorption (Fig. 3b), the composite exhibits a more sheet-like or flake-like morphology, indicating surface coverage by adsorbed phenol and possible structural rearrangement. Similarly, the MoS_2@GO composite before adsorption (Fig. 3c) shows compact aggregates with limited exfoliation. After phenol adsorption (Fig. 3d), the structure appears more transparent, suggesting enhanced dispersion and strong interfacial interaction between phenol molecules and the layered composite. The observed morphological changes after adsorption further support the successful interaction of phenol with the active surface of the prepared composites.

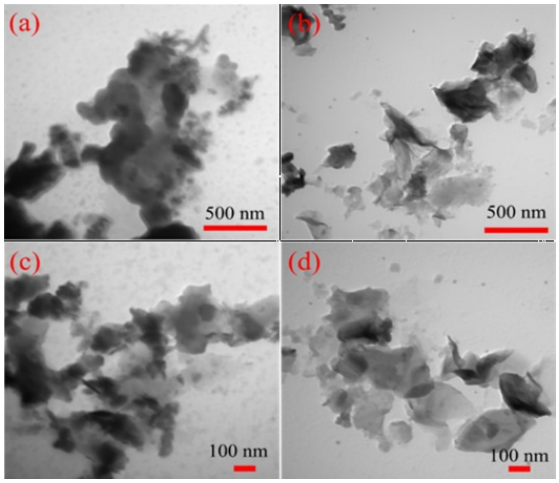

Fig. 3: TEM images of the synthesized MoS_2@C and MoS_2@GO composites before and after phenol adsorption: (a) MoS_2@C before adsorption, (b) MoS_2@C after adsorption, (c) MoS_2@GO before adsorption, and (d) MoS_2@GO after adsorption.

3.2 Adsorption Studies

3.2.1 Effect of pH

The effect of pH on phenol adsorption by C, MoS_2@C, and MoS_2@GO composites was investigated by varying the solution pH from 2 to 10 using a phenol concentration of 50 mg/L at 25 ∘C. As shown in Fig. 4, the highest phenol removal efficiency was achieved under strongly acidic conditions, and the adsorption efficiency gradually decreased with increasing pH. This behavior is attributed to the combined effects of phenol speciation and the surface chemistry of the adsorbents. At pH values below the pKa of phenol (≈9.9), phenol exists predominantly in its neutral molecular form (C_6H_5OH), which facilitates adsorption through π-π interactions between the aromatic ring of phenol and the carbonaceous surface, together with hydrogen bonding involving oxygen-containing surface functional groups. Under acidic conditions, protonation of the adsorbent surface also reduces the density of negatively charged surface sites, thereby favoring these intermolecular interactions. As the pH increases, phenol is progressively deprotonated to phenolate ions ($C_6H_5O^-$), while the adsorbent surface becomes increasingly negatively charged due to deprotonation of its functional groups [21]. Consequently, electrostatic repulsion between the negatively charged surface and phenolate ions, together with the stronger hydration of phenolate species, reduces the adsorption efficiency. Since the natural pH of the phenol solution was approximately 6, this pH was selected for all subsequent adsorption experiments.

3.2.2 Effect of initial phenol concentration

The effect of phenol concentration on the adsorption process was evaluated by varying the initial concentration in the range of 10-200 mg/L at 25 ∘C. Fig. 5a illustrates

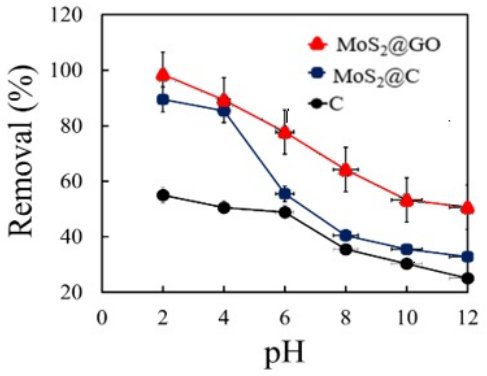

Fig. 4: Effect of pH on the removal efficiency. [m= 0.05 g, V = 20 mL; Co =50 mg/L, t = 25 ∘C].

how the three adsorbent materials (C, MoS_2@C, and MoS_2@GO) reduce phenol removal efficiency when the initial phenol concentration rises. Such reduced removal effectiveness can be explained by the fact that the number of adsorbent sites was fewer, producing a low surface area for adsorption and thus decreasing the adsorption efficiency. For C, MoS_2@C, and MoS_2@GO composites, the highest removal efficiency values were 59.31%, 88.73%, and 98.53%, respectively.

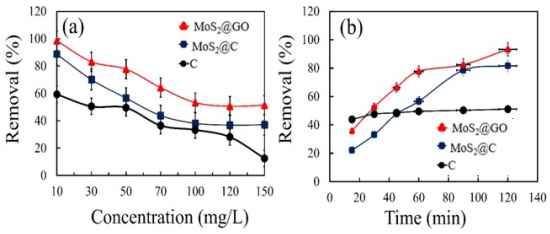

Fig. 5: Effect of (a) phenol concentration and (b) contact time on the removal efficiency. [m= 0.05 g, V = 20 mL; pH=6, Co =50 mg/L, t = 25 ∘C].

3.2.3 Effect of contact time

The influence of contact time on phenol adsorption was investigated, and the results are presented in Fig. 5b. The adsorption efficiency of phenol increased rapidly during the initial stage of the process due to the abundance of readily accessible active sites on the adsorbent surface. As the contact time increased, phenol molecules progressively diffused to these active sites and were adsorbed mainly through π-π interactions between the aromatic ring of phenol and the carbonaceous surface, together with hydrogen bonding and hydrophobic interactions. As adsorption proceeded, the number of available active sites gradually decreased because they became occupied by phenol molecules, resulting in a slower adsorption rate until equilibrium was reached. The MoS_2@GO composite exhibited the shortest equilibrium time among the investigated adsorbents, indicating faster adsorption kinetics, which can be attributed to its higher accessibility of active

sites and improved dispersion of the MoS_2 nanosheets on the GO support.

3.2.4 Effect of temperature

Fig. 6a illustrates the effect of temperature on phenol removal by our prepared samples. The experiments were performed by mixing 0.05 g of each adsorbent with 20 mL of phenol solution, with an initial concentration fixed at 50 mg/L. Then, the mixtures were kept under a magnetic stirrer for 90 min at a temperature range of 25 ∘C to 85 ∘C. As can be seen from Fig. 6a, the removal efficiency decreased with increasing temperature, which indicates that the adsorption of phenol is spontaneous and exothermic [22]. The partial loss of phenol molecules occurs due to the weakening of the physical link between the adsorbent and adsorbate with increasing temperature.

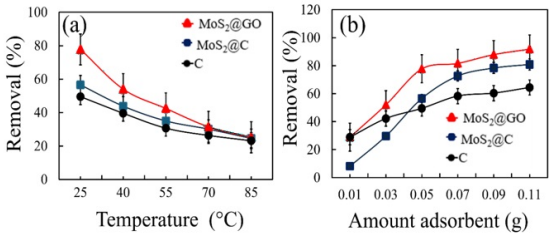

Fig. 6: Effect of (a) temperature and (b) amount of adsorbent on the removal efficiency. [pH=6, m= 0.05 g, V = 20 mL; Co =50 mg/L, temp: 25 ∘C].

3.2.5 Effect of adsorbent dose

Fig. 6b illustrates the effect of adsorbent dosage (0.01–0.11 g/20 mL) on the removal of phenol by C, MoS_2@C, and MoS_2@GO. For all adsorbents, the removal efficiency increased with increasing dosage due to the greater number of available adsorption sites and larger effective surface area. The enhancement was most pronounced between 0.01 and 0.05 g, where the removal efficiency increased rapidly. Beyond 0.05 g, only a slight increase was observed, indicating that most phenol molecules had already been adsorbed and that additional adsorption sites remained underutilized because of the limited phenol concentration. Throughout the investigated dosage range, MoS_2@GO exhibited the highest removal efficiency, reaching approximately 92% at 0.11 g, followed by MoS_2@C (≈80%) and C (≈64%). The superior performance of MoS_2@GO is attributed to the synergistic effect of GO and well-dispersed MoS_2 nanosheets, which provide a larger specific surface area and a higher density of accessible active sites for phenol adsorption. Considering both adsorption efficiency and adsorbent consumption, 0.05 g was selected as the optimum dosage for subsequent experiments.

3.2.6 Adsorption kinetics

Several kinetic models, specifically pseudo-first order and pseudo-second order models were used to investigate the kinetic behavior of phenol adsorption by C, MoS_2@C, and MoS_2@GO composites. The pseudo-first order (Eq. 3) and pseudo-second order (Eq. 4) mathematical expressions are as follows [23,24]:

$$\ln(q_e - q_t) = \ln q_e - k_1 t \tag{3}$$

$$\frac{t}{q_t} = \frac{t}{q_e} + \frac{1}{k_2 q_e^2} \tag{4}$$

Where, q_e (mg/g) is the adsorption capacity at equilibrium, k_1 (min^{-1}) and k_2 (g/(mg·min)) are the adsorption rate constants for pseudo-first order and pseudo-second order, respectively. t (min) is the contact time. The kinetic parameters presented in Table 1 indicate that the pseudo-second-order kinetic model provides a better fit to the experimental data for phenol adsorption onto the prepared composite materials, as evidenced by the higher correlation coefficient (R^2) values compared with those of the pseudo-first-order model (Fig. 7). This result suggests that the pseudo-second-order model more accurately describes the adsorption kinetics under the investigated experimental conditions. However, the kinetic fitting alone is insufficient to conclusively establish the adsorption mechanism. Therefore, the adsorption process is more appropriately attributed to the combined effects of π-π interactions, hydrogen bonding, and hydrophobic interactions between phenol molecules and the adsorbent surface, as discussed in the pH study, rather than solely to a chemisorption mechanism involving electron exchange [25,26].

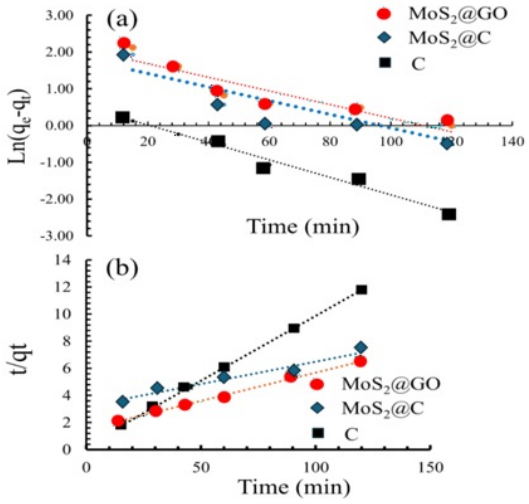

Fig. 7: Linearized plots of the pseudo-first-order (a) and pseudo-second-order (b) kinetic models for phenol adsorption onto C, MoS_2@C, and MoS_2@GO composites.

3.2.7 Adsorption isotherms

The adsorption isotherm is essential for explaining adsorbent-adsorbate interactions [24]. The Freundlich and Langmuir isotherm models are the most widely used isotherms to describe solid-liquid adsorption systems. The Langmuir isotherm model explains the adsorption of a single molecular layer onto a surface that contains a finite number of active sites [24,27]. This model assumes that

each site on the adsorbent surface has the same energy and that there are no interactions between adsorbed molecules. The Langmuir isotherm can be represented in its linear form by Eq. 5 [28].

$$\frac{C_e}{q_e} = \frac{C_e}{q_m} + \frac{1}{K_L q_m} \tag{5}$$

Where C_e (mg/L) is the equilibrium concentration, qmax (mg/g) is the maximum adsorbate amount, and K_L (L/mg) is the Langmuir constant related to the adsorption affinity of the binding sites. The Freundlich isotherm model effectively characterizes adsorption on heterogeneous surfaces that possess a variety of active sites with different energy levels [29]. It is based on the assumption that the amount of phenol adsorbed onto the surface is proportional to the equilibrium concentration of the solute in the solution, raised to a power denoted by the Freundlich exponent (n). The Freundlich isotherm is mathematically expressed by Eq. 6.

$$\log q_e = \log K_f + \frac{1}{n} \log C_e \tag{6}$$

Where qe and Ce are the same as those mentioned above in the Langmuir equation, K_f (L/g) and n are the Freundlich constants, which represent the adsorption capacity and intensity, respectively. The linear isotherm curves are shown in Fig. 8, and their parameters are listed in Table 2. As shown in Fig. 8, the adsorption of phenol best fits the Langmuir model ($R^2 > 0.99$), indicating the formation of a monolayer of phenol. In addition, the K_L values were in the range of 0.001–0.036, which implies favourable adsorption of phenol under the optimized parameters.

3.2.8 Thermodynamic analysis

The thermodynamic behaviors for the adsorption of phenol over the prepared materials were investigated. Gibbs free energy, $\Delta G\circ$ (kJ/mol), enthalpy change, $\Delta H\circ$ (kJ/mol), and entropy change, $\Delta S\circ$ (J/(mol·K)) were calculated using Eqs. 7-9 [22].

$$\Delta G^\circ = -RT \ln K_L \tag{7}$$

$$\Delta G^\circ = \Delta H^\circ - T\Delta S^\circ \tag{8}$$

$$\ln K_L = -\left[\frac{\Delta H^\circ}{RT}\right] + \left[\frac{\Delta S^\circ}{R}\right] \tag{9}$$

Where k_L is the distribution coefficient for adsorption, T is the absolute temperature, and R is the gas constant (8.314 J/(mol·K)). From the Van't Hoff plots (Fig. 9), the values of $\Delta H\circ$ and $\Delta S\circ$ were determined from the slope and intercept, respectively, while $\Delta G\circ$ was calculated using the thermodynamic relationship. As summarized in Table 3, the adsorption of phenol onto C, MoS_2@C, and MoS_2@GO is exothermic, as indicated by the negative $\Delta H\circ$ values (-1.233 to -1.873 kJ/mol). The relatively low magnitudes of $\Delta H\circ$ (<40 kJ/mol) suggest that the adsorption process is predominantly governed by physisorption [30]. The negative $\Delta S\circ$ values (-2.251 to -4.099 J/(mol·K)) indicate

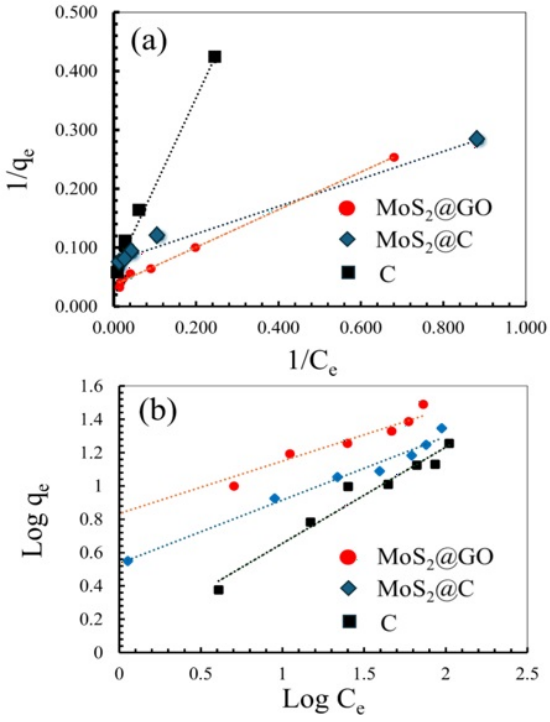

Fig. 8: Linear plots of the Langmuir (a) and Freundlich (b) adsorption isotherm models for phenol adsorption onto C, MoS_2@C, and MoS_2@GO composites.

a decrease in randomness at the solid-liquid interface due to the ordered arrangement of phenol molecules on the adsorbent surfaces [31]. The positive $\Delta G\circ$ values (0.669-1.466 kJ/mol) at all investigated temperatures indicate that the adsorption process is thermodynamically non-spontaneous under the studied conditions [32]. Moreover, the increase in $\Delta G\circ$ with increasing temperature suggests that adsorption becomes less thermodynamically favorable at higher temperatures, which is consistent with the exothermic nature of the adsorption process. Among the investigated adsorbents, MoS_2@GO exhibited the highest $\Delta G\circ$ and the most negative $\Delta S\circ$, indicating greater molecular ordering at the adsorbent surface.

3.2.9 The reusability of adsorbents

The reversibility of phenol adsorption and the regeneration performance of C, MoS_2@C, and MoS_2@GO adsorbents were evaluated using 0.1 M NaOH. As shown in Fig. 10, only a slight decline in removal efficiency was observed over five successive cycles, with MoS_2@GO retaining over 90% of its initial capacity, MoS_2@C about 80%, and C around 70%. The observed decrease is mainly due to the conversion of phenol into water-soluble sodium phenoxide upon interaction with NaOH, which promotes effective desorption. The regeneration efficiency of NaOH arises from three synergistic mechanisms: (1) hydrolysis of oxygenated surface groups and interaction with the hydroxyl group of phenol, (2) increased solubility of phenol in alkaline media, and (3) electrostatic repulsion between deprotonated acidic

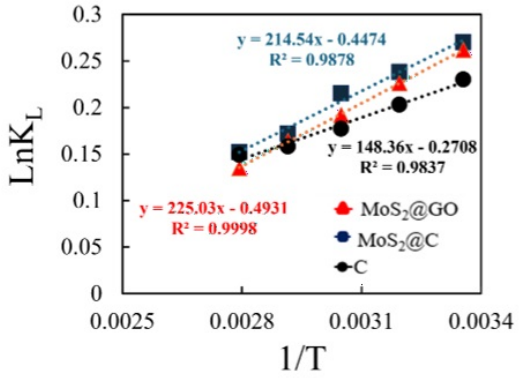

Fig. 9: Van't Hoff plots of phenol adsorption onto phenol over C, MoS_2@C, and MoS_2@GO composites.

groups on the adsorbent surface and adsorbed phenol [33]. These results demonstrate the excellent reusability and stability of the prepared adsorbents, underscoring their promise for sustainable and cost-effective wastewater treatment [33,34].

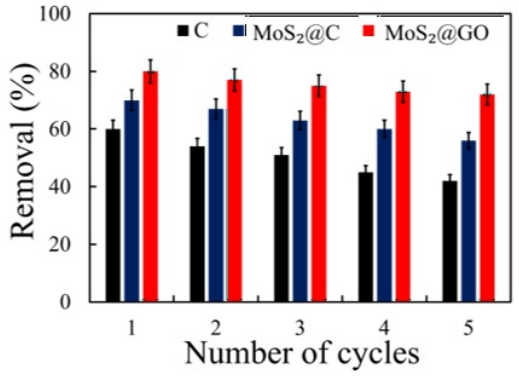

Fig. 10: Regeneration of C, MoS_2@C, and MoS_2@GO composites.

3.2.10 Proposed adsorption mechanism

The adsorption of phenol onto the prepared adsorbents is governed by the combined effect of multiple non-covalent interactions. Structural characterization confirmed that the MoS_2@GO composite possesses abundant oxygen-containing functional groups, graphitic domains, and well-dispersed MoS_2 nanosheets, providing numerous active adsorption sites. At the natural solution pH (≈6), phenol exists predominantly in its neutral form (pKa = 9.9), favoring adsorption through π-π interactions, hydrogen bonding, hydrophobic interactions, and weak van der Waals forces. The superior performance of the MoS_2@GO composite is attributed to the synergistic effect of GO and MoS_2, where GO provides a high surface area and abundant functional groups while preventing the aggregation of MoS_2 nanosheets. The pH-dependent adsorption behavior, together with the kinetic and thermodynamic results, supports this mechanism. Although the pseudo-second-order model best described the adsorption kinetics, it does not by itself imply chemisorption. Instead, the relatively low $\Delta H\circ$ values indicate that phenol adsorption is predominantly a physicochemical process governed mainly by physical interactions.

3.2.11 Comparison of phenol adsorption capacities

Table 4 compares the maximum adsorption capacity of the prepared MoS_2@GO composite with those of previously reported adsorbents for phenol removal. The prepared adsorbents exhibited maximum adsorption capacities ranging from 13.05 to 20.25 mg/g, with the MoS_2@GO composite showing the highest capacity (20.25 mg/g). This value is higher than those reported for several conventional and low-cost adsorbents, including GO-cellulose composites (6.20 mg/g), magnetic palm kernel biochar (10.84 mg/g), activated layered double hydroxide clay (12.00 mg/g), and natural clinoptilolite (7.98 mg/g). Recent studies have demonstrated that advanced graphene-based and functionalized carbon nanocomposites can achieve considerably higher adsorption capacities through enhanced surface area, tailored pore structure, and abundant oxygen-containing functional groups that promote π-π interactions, hydrogen bonding, and hydrophobic interactions with phenol molecules. Reported adsorption capacities include approximately 20.2 mg/g for GO, 23.47 mg/g for GO-coated biochar, 84 mg/g for poly(acrylic acid)-modified GO (GO-PAA), and over 190 mg/g for magnetic GO-based composites under optimized experimental conditions. Although the adsorption capacity of the present MoS_2@GO composite is lower than that of highly engineered graphene-based adsorbents, it remains competitive with many conventional materials while offering the advantages of a simple synthesis route, good structural stability, and improved surface functionality resulting from the synergistic combination of MoS_2 and GO. The incorporation of GO enhances the dispersion of MoS_2 nanosheets and increases the availability of active adsorption sites, facilitating phenol adsorption through π-π interactions, hydrogen bonding, and hydrophobic interactions. Therefore, the developed MoS_2@GO composite represents a promising adsorbent for phenol removal and compares favorably with many reported adsorbents while providing a cost-effective and facile alternative for wastewater treatment applications.

Table 1: Kinetic model parameters for phenol adsorption onto C, MoS_2@C, and MoS_2@GO composites.

Sample	Pseudo-first-order			Pseudo-second-order		
	q_e (mg/g)	k_1 (min^{-1})	R^2	q_e (mg/g)	k_2 (g/(mg·min))	R^2
C	0.46	0.00005	0.9808	10.45	0.0304	0.9990
MoS_2@C	5.97	0.00015	0.7075	30.21	0.0003	0.9490
MoS_2@GO	2.87	0.00017	0.8519	23.98	0.0012	0.9940

Table 2: Parameters of the Langmuir and Freundlich adsorption isotherm models for phenol adsorption onto C, MoS_2@C, and MoS_2@GO composites.

Sample	Langmuir model				Freundlich model	
	q_{max} (mg/g)	K_L (L/mg)	R^2	1/n	K_f (mg/g)(L/mg)$^{1/n}$	R^2
C	13.05	0.035	0.995	0.577	1.196	0.961
MoS_2@C	16.28	0.328	0.985	0.382	3.419	0.979
MoS_2@GO	20.25	1.860	0.997	0.315	6.841	0.981

Table 3: Thermodynamic parameters for the adsorption of phenol.

Adsorbents	$\Delta H\circ$ kJ/mol	$\Delta S\circ$ J/(mol.K)	$\Delta G\circ$ (kJ/mol)				
			298	313	328	343	358
C	-1.233	-2.251	0.669	0.703	0.737	0.771	0.805
MoS_2@C	-1.784	-3.720	1.108	1.162	1.218	1.274	1.330
MoS_2@GO	-1.873	-4.099	1.219	1.281	1.342	1.404	1.466

Table 4: Comparison of phenol adsorption capacities (q_{max}).

Adsorbent	q_{max} (mg/g)	Ref.
MoS_2@GO composite	20.25	This work
GO-cellulose composite	6.20	[35]
Magnetic palm kernel biochar	10.84	[36]
Activated layered double hydroxide clay	12.00	[37]
Clinoptilolite (natural zeolite)	7.98	[38]
Polyacrylic acid-modified graphene oxide (GO-PAA)	84.03	[39]
N-doped graphene oxide aerogel (NGOA)	108.19	[40]

4 Conclusion

The study confirmed that MoS_2@GO is an effective adsorbent for phenol, achieving 93% removal efficiency. Batch experiments assessing factors such as contact time, adsorbent dosage, initial phenol concentration, and temperature significantly influenced the adsorption process. Isotherm analysis showed strong linear correlations for both Langmuir and Freundlich models, indicating that phenol adsorption onto MoS_2@GO likely involve both monolayer coverage and heterogeneous surface interactions. Adsorption isotherms verified that the Langmuir isotherm model governed the adsorption of phenol onto C, MoS_2@C, and MoS_2@GO composites, with an estimated monolayer capacity of 13.05, 16.28, and 20.25 mg/g, respectively. The kinetic studies demonstrated that the adsorption process of phenol onto C, MoS_2@C, and MoS_2@GO composites followed the pseudo-second-order model, suggesting chemisorption. Thermodynamic analysis revealed that the adsorption of phenol was spontaneous and feasible, as indicated by the negative enthalpy change ($\Delta H\circ$), and the process was exothermic. Overall, the findings support the use of MoS_2@GO as a highly efficient, eco-friendly, and low-cost alternative to conventional methods for phenol removal from wastewater.

References

[1] Grégorio, C., Non-conventional low-cost adsorbents for dye removal: A review. Bioresource Technology, 2006. 97(9), 1061–1085 DOI: https://doi.org/10.1016/j.biortech.2005.05.001

[2] Abd-Ellatif, A.A.I.; Rashed, M.N.; Raslan, M.A.M.; Ali, S.G.; Ali, G.A.M., Removal of Fe(II) from aqueous solutions by Corchorus olitorius stem biochar as a cost-effective biosorbent. International Journal of Thin Film Science and Technology, 2026. 15(1), 117–131 DOI: https://doi.org/10.18576/ijtfst/150109

[3] Ahmed, S.S.; Abdulghafar, B.A.; Abdullah, H.M.; Yasin, S.A.; Jabar, R.S.A.; Chong, K.F.; Ali, G.A.M.; Bakr, Z.H., Photocatalytic degradation of Cr(VI) via electrospun MWCNTs-Fe_3O_4@PET and MWCNTs-Fe_3O_4/PET nanofibers. International Journal of Thin Film Science and Technology, 2026. 15(1), 65–73 DOI: https://doi.org/10.18576/ijtfst/150105

[4] Duan, W.; Meng, F.; Cui, H.; Lin, Y.; Wang, G.; Wu, J., Ecotoxicity of phenol and cresols to aquatic organisms: A review. Ecotoxicology and Environmental Safety, 2018. 157, 441–456 DOI: https://doi.org/10.1016/j.ecoenv.2018.03.089

[5] Ahmaruzzaman, M.; Mishra, S.R.; Gadore, V.; Yadav, G.; Roy, S.; Bhattacharjee, B.; Bhuyan, A.; Hazarika, B.; Darabdhara, J.; Kumari, K., Phenolic compounds in water: From toxicity and source to sustainable solutions – An integrated review of removal methods, advanced technologies, cost analysis, and future prospects. Journal of Environmental Chemical Engineering, 2024. 12(3), 112964 DOI: https://doi.org/10.1016/j.jece.2024.112964

[6] Zheng, T.-H.; Zhang, Z.-Z.; Liu, Y.; Zou, L.-H., Recent progress in catalytically driven advanced oxidation processes for wastewater treatment. Catalysts, 2025. 15(8), 761 DOI: https://doi.org/10.3390/catal15080761

[7] Saputera, W.H.; Putrie, A.S.; Esmailpour, A.A.; Sasongko, D.; Suendo, V.; Mukti, R.R., Technology advances in phenol removals: current progress and future perspectives. Catalysts, 2021. 11(8), 998 DOI: https://doi.org/10.3390/catal11080998

[8] Mohammed, A.E.; Abdullah, G.H.; Yousif, S.H.; Humadi, J.I., Catalytic degradation of phenol from refinery wastewater using hybrid oxidation-adsorption in multi fixed-bed reactor: Experimental and kinetic study. Journal of Water Process Engineering, 2026. 83, 109558 DOI: https://doi.org/10.1016/j.jwpe.2026.109558

[9] Magne, P.; Walker, P.L., Phenol adsorption on activated carbons: Application to the regeneration of activated carbons polluted with phenol. Carbon, 1986. 24(2), 101–107 DOI: https://doi.org/10.1016/0008-6223(86)90102-8

[10] Teweldebrihan, M.D.; Gnaro, M.A.; Dinka, M.O., Adsorption of phenol from aqueous solution utilizing activated carbon prepared from cathaedulis stem. Environments, 2025. 12(9), 314 DOI: https://doi.org/10.3390/environments12090314

[11] Darweesh, R.F.H.; Zaki, R.M.; Mahdy, A.; Ahmed, A.S.A., Enhanced adsorption of methylene blue (MB) dye by the MoS_2/ZIF-8 composite: isotherm and kinetics studies. Materials Advances, 2026. 7(1), 338–350 DOI: https://doi.org/10.1039/D5MA00636H

[12] Yousef, D.; Ahmed, A.S.A.; Hamed, A.M.; Abdelmotallieb, M.; El-Sayed, M.E.A., Enhanced wastewater purification using biochar, activated carbon, and kaolinite composites: a multi-parameter approach for sustainable agriculture. Sustainability, 2026. 18(8), 3696 DOI: https://doi.org/10.3390/su18083696

[13] Ali, A.F.M.; Ahmed, A.S.A.; Gahlan, A.A.; El-sayed, A.-A.Y., Biochar derived from peanut husks as an adsorbent to ammonium ions remediation from aqueous solutions. Egyptian Journal of Chemistry, 2024. 67(12), 231–244 DOI: https://doi.org/10.21608/ejchem.2024.271974.9374

[14] Tolan, D.; El-Sawaf, A.; Ahmed, A.S.A.; Nassar, A.; Mohamed, N.M.; Alhindawy, I.G.; Elshehy, E.A.; Utgikar, V., Enhanced photocatalytic activity of (In–Sr–P) tridoped TiO_2/Bi_2O_3 composite loaded on mesoporous carbon: A facile sol-hydrothermal synthesis approach. Materials Chemistry and Physics, 2024. 322, 129570 DOI: https://doi.org/10.1016/j.matchemphys.2024.129570

[15] Ngeno, E.C.; Mbuci, K.E.; Necibi, M.C.; Shikuku, V.O.; Olisah, C.; Ongulu, R.; Matovu, H.; Ssebugere, P.; Abushaban, A.; Sillanpää, M., Sustainable re-utilization of waste materials as adsorbents for water and wastewater treatment in Africa: Recent studies, research gaps, and way forward for emerging economies. Environmental Advances, 2022. 9, 100282 DOI: https://doi.org/10.1016/j.envadv.2022.100282

[16] Thabet, I.K.M.; Ahmed, A.S.A.; Ali, G.A.M.; Bakr, Z.H.; Hamed, A.M.; Nagiub, A.M., Highly efficient Co_3O_4/GO adsorbent recycled from spent Lithium-Ion Batteries toward cationic dye from aqueous solutions. Egyptian Journal of Chemistry, 2025. 68(13), 1053–1064 DOI: https://doi.org/10.21608/ejchem.2025.364725.11379

[17] Bishnoi, P.; Chauhan, G.; Hart, P.; Siwal, S.S.; Thakur, V.K., Next-generation water treatment with molybdenum disulfide: dual-functionality in pollutant adsorption and photocatalysis. Advanced Materials Technologies, 2026, e02557 DOI: https://doi.org/10.1002/admt.202502557

[18] Ali, Z.; Hussain, Q.; Yawer, M.A.; Mehmood, M.; Hussain, R.; Shah, A.; Kanwal, H.; Yawer, A.; Ahmad, S.; Zahid, S., Effect of sulfur precursors on hydrothermal growth of MoS_2 nanostructures and its visible-light-driven photocatalytic activities. Journal of Molecular Structure, 2023. 1278, 134929 DOI: https://doi.org/10.1016/j.molstruc.2023.134929

[19] Huang, H.; Liu, N.; Wang, X.; Luo, Q.; Huang, X.; Wang, X.; Zhong, M.; Zhang, H., DFT calculation of hydrothermal mechanism on preparation of MoS_2. Journal of Molecular Modeling, 2020. 26(10), 257 DOI: https://doi.org/10.1007/s00894-020-04521-2

[20] Zhang, J.; Han, D.; Wang, Y.; Wang, L.; Chen, X.; Qiao, X.; Yu, X., Synergy between nanozymes and natural enzymes on the hybrid MoS_2 nanosheets/graphite microfiber for enhanced voltammetric determination of hydrogen peroxide. Microchimica Acta, 2020. 187(6), 321 DOI: https://doi.org/10.1007/s00604-020-04299-3

[21] Wong, S.; Ghafar, N.A.; Ngadi, N.; Razmi, F.A.; Inuwa, I.M.; Mat, R.; Amin, N.A.S., Effective removal of anionic textile dyes using adsorbent synthesized from coffee waste. Scientific Reports, 2020. 10(1), 2928 DOI: https://doi.org/10.1038/s41598-020-60021-6

[22] Althomali, R.H.; Alamry, K.A.; Hussein, M.A.; Guedes, R.M., An investigation on the adsorption and removal performance of a carboxymethylcellulose-based 4-aminophenazone@MWCNT nanocomposite against crystal violet and brilliant green dyes. RSC Advances, 2023. 13(7), 4303–4313 DOI: https://doi.org/10.1039/D2RA07321H

[23] Zhu, H.Y.; Jiang, R.; Xiao, L.; Zeng, G.M., Preparation, characterization, adsorption kinetics and thermodynamics of novel magnetic chitosan enwrapping nanosized γ-Fe_2O_3 and multi-walled carbon nanotubes with enhanced adsorption properties for methyl orange. Bioresource Technology, 2010. 101(14), 5063–5069 DOI: https://doi.org/10.1016/j.biortech.2010.01.107

[24] Mallakpour, S.; Naghdi, M., Design and identification of poly(vinyl chloride)/layered double hydroxide@MnO_2 nanocomposite films and evaluation of the methyl orange uptake: linear and non-linear isotherm and kinetic adsorption models. New Journal of Chemistry, 2020. 44(16), 6510–6523 DOI: https://doi.org/10.1039/D0NJ01162B

[25] Bibi, A.; Sayadi, S.; Abu-Dieyeh, M.; Zouari, N.; Al-Ghouti, M.A., Adsorption of phenol and bisphenol-A by activated carbon and graphene oxide: a comparative study. Environmental Science and Pollution Research, 2025. 32(50), 28840–28863 DOI: https://doi.org/10.1007/s11356-025-37204-7

[26] Anisuzzaman, S.M.; Joseph, C.G.; Krishnaiah, D.; Bono, A.; Suali, E.; Abang, S.; Fai, L.M., Removal of chlorinated phenol from aqueous media by guava seed (Psidium guajava) tailored activated carbon. Water Resources and Industry, 2016. 16, 29–36 DOI: https://doi.org/10.1016/j.wri.2016.10.001

[27] Langmuir, I., The Constitution and Fundamental Properties of Solids and Liquids. Part I. Solids. Journal of the American Chemical Society, 1916. 38(11), 2221–2295 DOI: https://doi.org/10.1021/ja02268a002

[28] Al-Saeedi, S.I.; Areej, A.; Qamar, M.T.; Alhujaily, A.; Iqbal, S.; Alotaibi, M.T.; Aslam, M.; Qayyum, M.A.; Bahadur, A.; Awwad, N.S.; Jazaa, Y.; Elkaeed, E.B., Isotherm and kinetic studies for the adsorption of methylene blue onto a novel Mn_3O_4-Bi_2O_3 composite and their antifungal performance. Frontiers in Environmental Science, 2023. 11, 1156475 DOI: https://doi.org/10.3389/fenvs.2023.1156475

[29] Freundlich, H., Über die adsorption in lösungen. Zeitschrift für physikalische Chemie, 1907. 57(1), 385–470 DOI: https://doi.org/10.1515/zpch-1907-5723

[30] Tran, H.N.; Lima, E.C.; Juang, R.-S.; Bollinger, J.-C.; Chao, H.-P., Thermodynamic parameters of liquid–phase adsorption process calculated from different equilibrium constants related to adsorption isotherms: A comparison study. Journal of Environmental Chemical Engineering, 2021. 9(6), 106674 DOI: https://doi.org/10.1016/j.jece.2021.106674

[31] Elousta, O.S.; Aboeleneen, N.; Monem, N.A.; Farrag, T.I., Phenol removal from aqueous solutions using date pits as a natural adsorbent. Port-Said Engineering Research Journal, 2026. 30(1), 112–120 DOI: https://doi.org/10.21608/pserj.2025.410561.1432

[32] Ahmed, A.S.A.; Haggag, E.S.A.; Cheira, M.F.; Abdelsamad, A.A.; Abdel-lateef, A.M., Rapid synthesis of phosphomolybdic acid encapsulated ZIF-8 for efficient uranium(vi) capture from alkaline solution. RSC Advances, 2025. 15(43), 36365–36379 DOI: https://doi.org/10.1039/D5RA06854A

[33] Lingamdinne, L.P.; Angaru, G.K.R.; Pal, C.A.; Koduru, J.R.; Karri, R.R.; Mubarak, N.M.; Chang, Y.-Y., Insights into kinetics, thermodynamics, and mechanisms of chemically activated sunflower stem biochar for removal of phenol and bisphenol-A from wastewater. Scientific Reports, 2024. 14(1), 4267 DOI: https://doi.org/10.1038/s41598-024-54907-y

[34] Mohan, B.; Girish, C.R.; Jeppu, G.; Patil, P., Bauhinia monandra derived mesoporous activated carbon for the efficient adsorptive removal of phenol from wastewater. Scientific Reports, 2025. 15(1), 31790 DOI: https://doi.org/10.1038/s41598-025-17444-w

[35] Kumar, N.; Kumar, B.; Gupta, H.; Kumar, A., Development and evaluation of cellulose/graphene-oxide based composite for removing phenol from aqueous solutions. Polymers, 2023. 15(3), 572 DOI: https://doi.org/10.3390/polym15030572

[36] Hairuddin, M.N.; Mubarak, N.M.; Khalid, M.; Abdullah, E.C.; Walvekar, R.; Karri, R.R., Magnetic palm kernel biochar potential route for phenol removal from wastewater. Environmental Science and Pollution Research, 2019. 26(34), 35183–35197 DOI: https://doi.org/10.1007/s11356-019-06524-w

[37] Tabana, L.; Tichapondwa, S.; Labuschagne, F.; Chirwa, E., Adsorption of phenol from wastewater using calcined magnesium-zinc-aluminium layered double hydroxide clay. Sustainability, 2020. 12(10), 4273 DOI: https://doi.org/10.3390/su12104273

[38] Uçar, S.; Evcin, A.; Uçar, M.; Alibeyli, R.; Majdan, M., Removal of phenol and chlorophenols from aquatic system using activated clinoptilolite. Hacettepe Journal of Biology and Chemistry, 2015. 43(3), 235–249 DOI: https://doi.org/10.15671/HJBC.20154314246

[39] Bibi, A.; Bibi, S.; Abu-Dieyeh, M.; Al-Ghouti, M.A., New material of polyacrylic acid-modified graphene oxide composite for phenol remediation from synthetic and real wastewater. Environmental Technology and Innovation, 2022. 27, 102795 DOI: https://doi.org/10.1016/j.eti.2022.102795

[40] Cui, Y.; Kang, W.; Hu, J., Effectiveness and mechanisms of the adsorption of phenol from wastewater onto N-doped graphene oxide aerogel. Journal of Water Process Engineering, 2023. 53, 103665 DOI: https://doi.org/10.1016/j.jwpe.2023.103665